Computing and Informatics, Vol. 44, 2025, 1423–1444, doi: 10.31577/cai_2025_6_1423

OBJECT-BASED HYPERSPECTRAL CLASSIFICATION APPROACH TO TREE SPECIES BY 3D-CNN

Radoslav Forgáč, Bianca Badidová, Miloš Očkay, Martin Javurek, Ladislav Hluchý

Institute of Informatics
Slovak Academy of Sciences
Dúbravská cesta 9
845 07 Bratislava, Slovakia
e-mail: {radoslav.forgac, bianca.badidova, milos.ockay, martin.javurek, ladislav.hluchy}@savba.sk

Ľuboš Skurčák

Department of Science, Research, Development and Analysis
VUJE, a.s.
Okružná 5
918 64 Trnava, Slovakia
e-mail: lubos.skurcak@vuje.sk

Abstract. This article focuses on the design and implementation of a 3D Convolutional Neural Network (3D-CNN) for hyperspectral classification of tree species. Real data from repeated aerial imaging of selected sections of the Slovak electricity transmission system was used to test the models, using technology from our partner VUJE, a.s., which has a hyperspectral scanner consisting of two cameras, HySpex VNIR-1800 and HySpex SWIR-384, capturing wavelengths from 400 to 2 500 nm. The results of 3D-CNN classification based on autumn and spring data collection were compared, as well as classification after fusing data from selected areas for the purpose of comparing object vs. pixel classification. The presented object-based classification model based on 3D-CNN achieves on average 9 % better classification accuracy compared to pixel-based classification using a 1D Convolutional Neural Network (1D-CNN).

Keywords: Hyperspectral image classification, 3D convolutional neural network, object-based classification, dimensionality reduction, feature extraction

1 INTRODUCTION

Currently, significant progress is being observed worldwide in remote data acquisition using hyperspectral imaging technology. Given the current possibilities, it is safe to say that hyperspectral imaging is ready for applications focused on remote sensing. Hyperspectral imaging is currently used in areas like agriculture, mineral exploration, environmental monitoring, and electrical power engineering. Our interest focused on the use of this technology in the power industry. Its application in this area can increase the reliability of power line structures as critical infrastructure. In real-world operations, trees growing near power lines can cause power transmission and distribution outages during adverse weather conditions, resulting in significant economic damage. Early diagnosis can significantly help to prevent such outages. However, given the extent of power networks, this task is challenging, as in Slovakia alone, for example, the total length of transmission lines exceeds 2400 km, and the total length of 110 kV lines exceeds 6732 km. It has been confirmed that aerial surveys are practically the only effective way to obtain the necessary information about the condition of power lines.

The authors' goal was to design artificial intellingence (AI) models for classifying tree species using hyperspectral images taken during aerial surveys of overhead power lines in Visolaje, Sverepec, Závada, and Počarová. During the project, 28 flights were carried out by the project partner VUJE, a.s. Approximately 550 GB of data was obtained from each flight, totalling 15 TB of data for further processing. The importance of aerial surveys increases when they are accompanied by aerial scanning using the latest diagnostic systems capable of scanning across a wide range of wavelengths and providing digital data even outside the visible spectrum, which has the potential to detect operational threats at an early stage.

The rest of the paper is organized as follows. Section 2 provides an overview of related work in hyperspectral data processing with a focus on dimensionality reduction and classification approaches. Section 3 describes the hyperspectral data collection of three selected areas in Slovakia regions: Visolaje, Sverepec and Počarová, especially for the autumn and spring data collection. Section 4 presents the theoretical background and architectural details of the 3D-CNN. Section 5 describes the experiments including data preprocessing and proposed models training. Finally, Section 6 provides the results of comparing classifications from autumn and spring data collections as well as a comparison of the classification accuracy of 3D-CNN and 1D-CNN.

2 RELATED WORK

From a research perspective, the processing and analysis of hyperspectral data have increased significantly in recent years [1, 2, 3]. Classification has become one of the main areas of focus in analyzing hyperspectral data. When classifying this type of data, dimensionality becomes a major challenge due to the large number of spectral bands it contains [4]. Therefore, reducing the dimensionality of hyperspectral channels is essential for achieving accurate classification results.

2.1 Dimensionality Reduction

Dimensionality reduction can be divided into two main groups in terms of hyperspectral data. The first group deals with feature extraction, a process commonly used in conventional image analysis, although in hyperspectral data, it involves the extraction of features across a much higher number of spectral bands [5, 6, 7, 8], and the second focuses on the selection of relevant bands [9, 10, 11].

The concept of feature extraction involves transforming the original feature space into a new one. The disadvantage is the loss of the physical interpretability of the bands. However, more information is stored in the new feature space. The selection of features from the original bands works with predefined criteria, based on which the relevant bands are selected [12]. Unlike feature extraction, feature selection preserves the physical interpretability of the bands, but the information contained in the bands that were not selected is no longer preserved. Feature extraction methods can be divided into three groups based on the nature of the analyzed domain. The first two groups consist of spectral [13] and spatial [14] extraction methods that focus on individual domains separately. Their disadvantage is that they ignore the common spectral-spatial correlation. The third group consists of spectral-spatial feature extraction methods [15, 16, 17], which integrate spatial information with spectral information in order to achieve better results. In this case, the spatial properties of pixels are often extracted using their local neighborhood pixels, thereby extracting elements from both the spectral and spatial domains simultaneously. This eliminates the disadvantage of extracting features from individual domains separately, thereby preserving the original spectral-spatial correlation [18].

Study [12] divides feature selection into three categories. The first category is further divided based on the evaluation of a subset of bands and includes filter methods [19, 20, 21], wrapper methods [22, 23], and hybrid methods [24, 25]. Filter methods use selection criteria independent of the classifiers used. Wrapper methods select bands based on the classification performance of the classifier. Hybrid feature selection methods combine these two methods.

There are two subgroups based on the feature selection strategy used, depending on the number of bands analyzed. The first is individual band evaluation. This subgroup is based on evaluating the importance (score) of individual bands according to specific criteria. Techniques such as ranking [19] and clustering [20] are often used in this context. The second subgroup is the evaluation of subsets of bands,

where candidate subsets of bands are created using search strategies. These include algorithms such as exhaustive and greedy search [21, 24] as well as combinatorial or metaheuristic optimization methods [22, 23, 25].

2.2 Classification Approaches

In terms of classification, we distinguish between approaches based on the analyzed domain. These are either spectral classification, where a single pixel containing a unique spectral signature is provided as an input to the classifier. This type of classification is also called pixel classification. The second type of approach is object classification methods, where the classifier works with sets of pixels representing individual objects that contain spatial information in addition to spectral information. Machine learning approaches, especially neural networks, are widely used in the pixel classification of hyperspectral data, such as the Multilayer Perceptron (MLP) [26] and 1D-CNN [27].

In most cases, classification models that use spectral signatures of individual pixels without spatial information for training perform worse than models that use object-based classification. The reason for this is the very limited information contained in a single spectrum. Maintaining object continuity is challenging, which often leads to misclassification of pixels belonging to the same class [28]. Similar to pixel classification, current studies on object classification of hyperspectral data mainly use approaches from the field of machine learning. The most common methods used here are 3D-CNN [29] and random forest [30].

3 HYPERSPECTRAL DATA COLLECTION

Hyperspectral data were obtained with the assistance of VUJE a.s. and the Technical University of Zvolen (TUZVO). The data was obtained by aerial mapping, using two hyperspectral cameras, namely HySpex VNIR-1800 and HySpex SWIR-384. These cameras are designed to capture a wavelength range of 400 to 2 500 nm. The results of this scanning were hyperspectral recordings in the range of 400 to 1 000 nm for the HySpex VNIR-1800 camera, with a maximum sampling range of 3.26 nm per spectral channel and a grayscale dynamic range of at least 20k. HySpex SWIR-384 recorded wavelengths in the 980 to 2 500 nm range using a high-end sensor cooled to 150°K, which achieves low background noise and a high dynamic range. The system achieves excellent image quality in darker areas of highly dynamic scenes due to its high optical transmittance (f/2.0), aberration-corrected optics, and a maximum frame rate of 400 frames per second. The next step involved annotating the acquired data. To ensure the highest possible accuracy of the reference labels, the annotation process was supported by ground campaign, during which each area was physically visited. It also included the selection of the tree species of interest, where their condition and suitability for use of their hyperspectral characteristics were assessed. After the preprocessing, the data is entered into the tree database,

where each pixel of the trees of interest is described. For the purpose of this paper, preprocessing included band selection, where the first 186 hyperspectral bands were selected (HySpex VNIR-1800 range) [31].

The database contains:

- a unique area represented by the area number,
- the local name of the area,
- the sequence number of the tree species within the area represented by the tree species number,
- unique object within the area represented by the object id,
- the species of tree, the name or abbreviation of the tree,
- damage, which indicates the degree of damage to the tree species,
- the date of the aerial survey,
- the position of each pixel in space specified by the X and Y coordinates,
- 186 channels, representing radiance values.

The dataset was acquired from four regions in Slovakia: Visolaje, Sverepec, Počarová, and Závada. Three of these regions were selected for the experiments: Visolaje, Sverepec, and Počarová. Závada was omitted due to the low representation of samples of individual tree species for the chosen collections and the higher number of missing values, which could cause significant deviations. Two airborne data acquisitions were used in this study, conducted on November 3, 2022 (autumn) and April 18, 2023 (spring) (Table 1). The hyperspectral data obtained by the airborne campaign carry information about the radiance across different parts of the spectrum. This information is captured across 186 channels (Columns b1 to b186). Based on this, it is possible to plot spectral characteristics for each pixel within the area, these are shown in Figure 1. The depicted spectral characteristics belong to four selected tree species from the Sverepec area. A considerable variability of individual values in each channel for the tree species is present. For this reason, Principal Component Analysis (PCA) is used in this work to extract features, which, despite increased variability within a single class, is able to extract relevant information [32].

From the data stored in the tree database, we can reveal the location of individual trees in specific areas. For comparison of the displays of individual trees shown based on the information from the database, we also attach real images of the areas of interest (Figure 2). By comparing the actual images and the rendered tree objects in each area, a significant reduction in the number of objects in each area is visible.

This proves that the data was corrected and cleaned. Not all the trees were marked and labelled. Removal of the inappropriate radiance values in the different parts of the spectrum caused by inappropriate illumination of the objects or shading of the objects was performed. Also, the physical inspection of the surveyed area

Abbr.	Tree Species	Visolaje		Počarová		Sverepec	
		aut. 2022	**spr. 2023**	**aut. 2022**	**spr. 2023**	**aut. 2022**	**spr. 2023**
AC	Acer campestre	8 001	10 997	730	730	1 209	1 101
AG	Alnus glutinosa	7 986	7 858	1 782	1 233		
APl	Acer platanoides	339	339				
APs	Acer pseudoplatanus			245	201	1 865	268
BS	Betula sp.	1 167	482	658	531		
BV	Berberis vulgaris					33	
CA	Corylus avellana	1 216	959	402	337	1 374	1 323
CB	Carpinus betulus	2 446	2 460	1 738	79	959	870
CM	Crataegus monogyna	269	269			190	179
CS	Cerasus sp.			5 050	4 709		
FA	Frangula alnus			31	31		
FS	Fagus sylvatica					4 408	3 945
LD	Larix decidua					1 834	1 719
PA	Picea abies	24 253	18 963	21 990	15 863	1 987	1 746
PC	Pyrus communis	851	810				
PP	Prunus padus			199	295		
Pr	Prunus	833	843				
PSy	Pinus sylvestris	8 547	8 642				
PSp	Prunus spinosa			46	33	681	657
PT	Populus tremula			8 601	9 563	51	85
QP	Quercus petraea			130	131		
QR	Quercus robur	9 499	5 684	9 513	8 042		
SA	Salix alba		313				
SCi	Salix cinerea	464	4 037	268	232		
SCa	Salix caprea	387	3 769	920	767	104	102
SN	Sambucus nigra			252	250		
SS	Swida sanguinea		116				
TC	Tilia cordata	682	677	1 439	1 335		
28	**overall**	**66 940**	**67 218**	**53 994**	**44 362**	**14 695**	**11 995**

Table 1. Pixel distribution of autumn 2022 and spring 2023 data collection for each tree species in the Visolaje, Pocarova, and Sverepec area

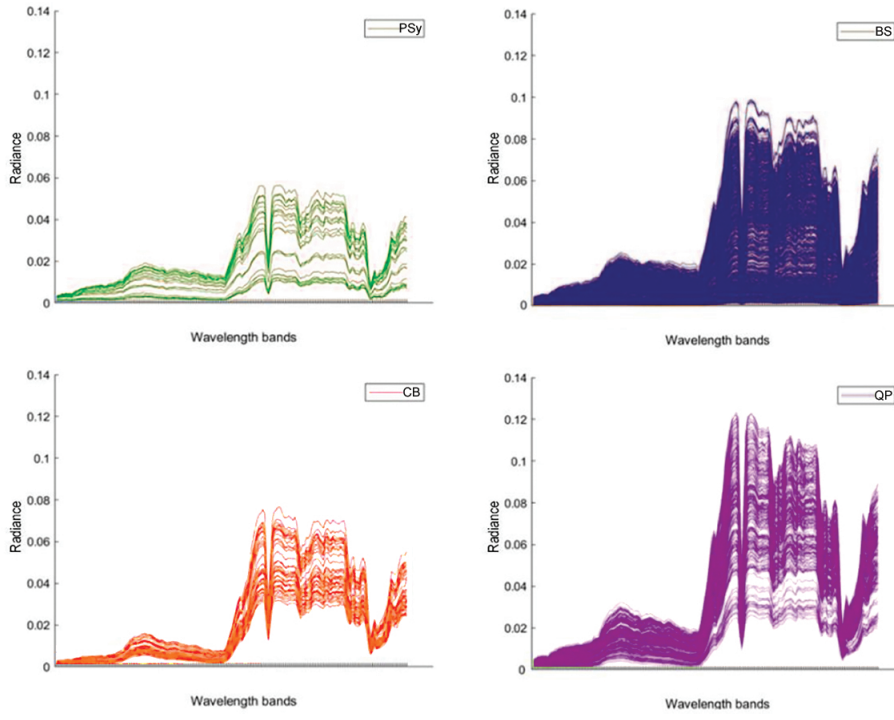

Figure 1. Spectral characteristics of selected tree species from the Sverepec area

resulted in the reduction of objects that are not suitable for further processing. Thus, individual aerial data collections contain different numbers of individual tree species as well as tree objects, and thus individual pixel content at given areas. Individual areas from a single aerial collection are shown in Figures 3, 4, and 5).

Figure 2. Real images of the areas of interest

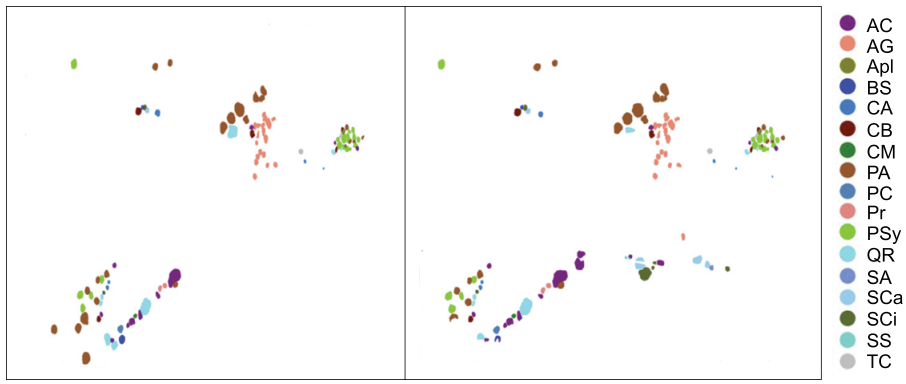

Figure 3. Visolaje area, left – autumn 2022 and right – spring 2023

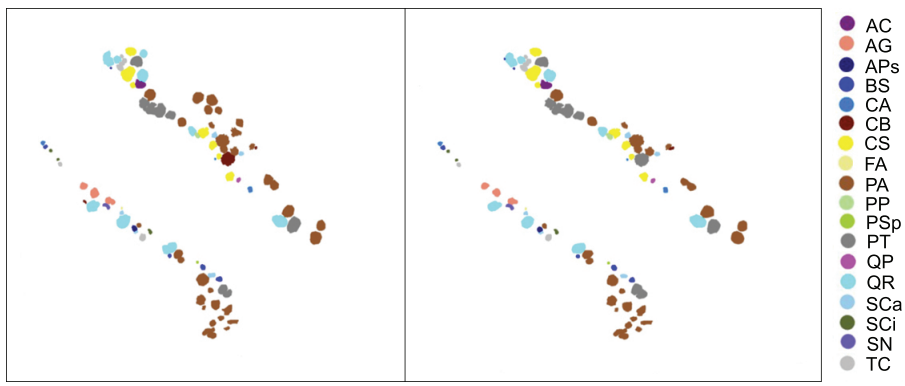

Figure 4. Sverepec area, left – autumn 2022 and right – spring 2023

Each area contains a different number of tree species with different numbers of pixels for separate objects. This is mainly due to the size of the crowns of each tree species. Also, the abundance of individual trees in the same area may differ, which is due to the time interval between the flights and also the change in foliage in autumn and spring.

In terms of pixel count, the Visolaje area is the most numerous. It contains 15 different species of trees which are made up of a total of 66 940 pixels, in autumn only. In contrast, in the spring, the Visolaje area contains 17 species of trees, made up of a total of 67 218 pixels (Figure 6). The new tree species that were not present in the autumn collection are 'Salix alba' and 'Swida sanguinea'. This is due to the exclusion of these tree species in the autumn, as they did not provide relevant hyperspectral characteristics at the time of the aerial survey and subsequent ground campaign. It is visible that they form a relatively small set of pixels, with "Salix alba" consisting of 313 pixels, and "Swida sanguinea" with only 116 pixels. The

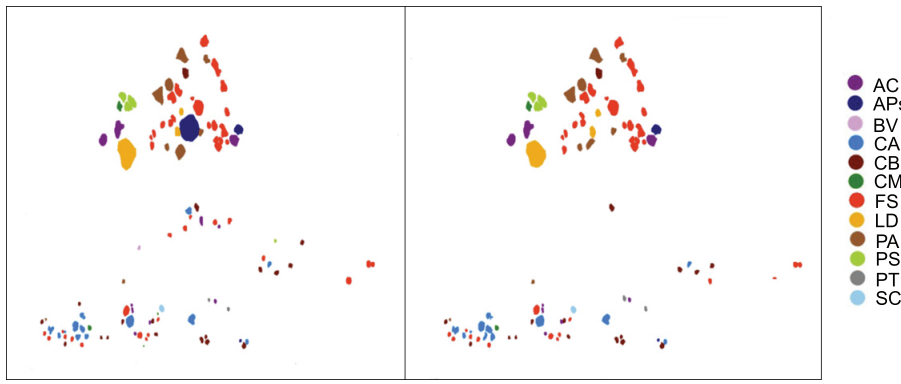

Figure 5. Počarová area, left – autumn 2022 and right – spring 2023

most abundant tree species in both collections, represented by the largest number of pixels, is "Picea abies". It is represented by 24 253 pixels in the autumn and 18 963 pixels in the spring. We can observe a difference in the abundance of the same tree species in autumn and spring. This difference is mainly due to changes in foliage and possible changes in the canopy that may have occurred due to weather conditions or human influence.

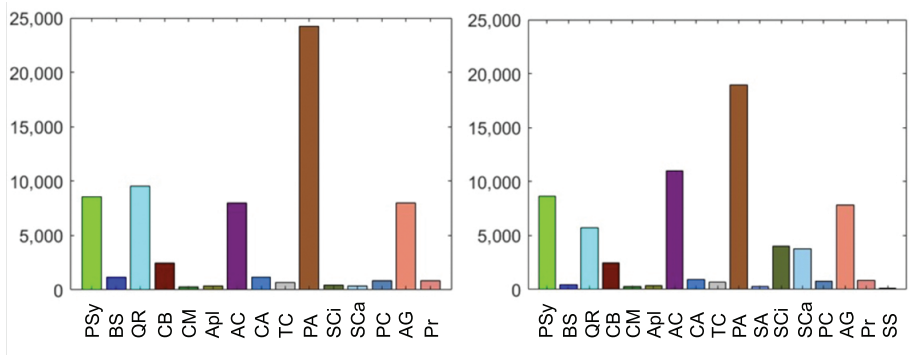

Figure 6. Number of pixels for individual tree species in the Visolaje area, left – autumn 2022 and right – spring 2023

In terms of different tree species, the most numerous area is Sverepec. This area contains the same number of different tree species both in the autumn and spring (Figure 7). There are 18 different tree species. The most abundant tree species, as in the Visolaje area, is "Picea abies". This tree species was represented by 21 990 pixels in the autumn and 15 863 pixels in the spring. In total, this area contains 53 994 individual pixels in autumn and 44 362 pixels in the spring.

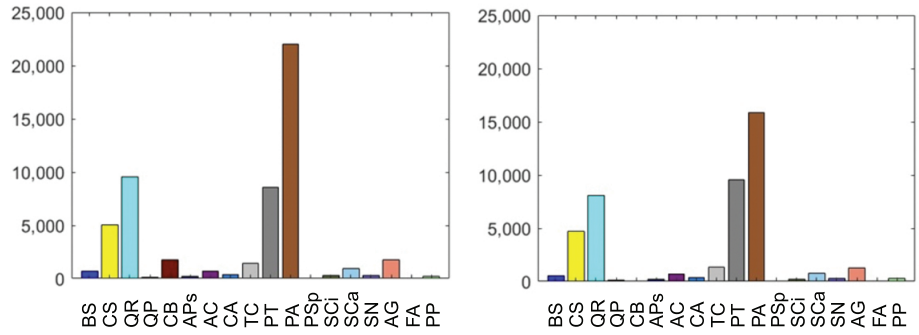

Figure 7. Number of pixels for individual tree species in the Sverepec area, left – autumn 2022 and right – spring 2023

The Počarová area has the smallest number of different tree species. It contains 12 different tree species in the autumn and only 11 different tree species in the spring (Figure 8). The tree species that is missing from the spring collection is "Berberis vulgaris". We assume that this tree species has been removed due to damage. In the autumn, there were only 33 pixels containing spectral signatures of this tree species. The most abundant tree species in terms of pixels in the autumn is 'Fagus sylvatica' with 4 408 pixels. In the spring, the most abundant tree species is again 'Fagus sylvatica', which contains 3 945 pixels. In total, the autumn collection contains 14 695 individual pixels. The spring collection contains 11 995 pixels.

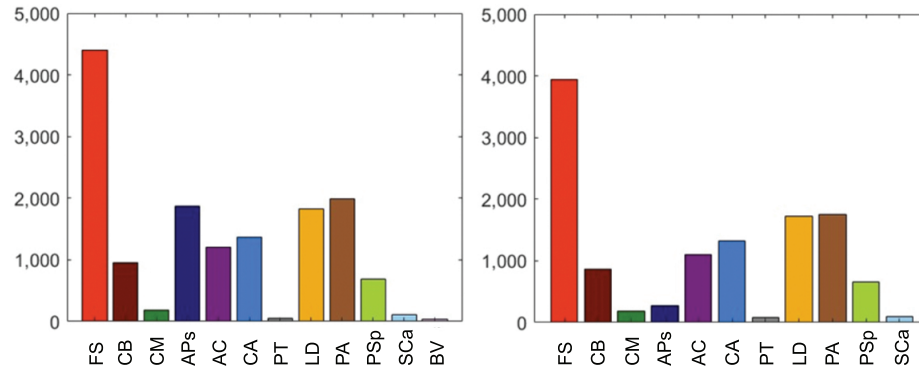

Figure 8. Number of pixels for individual tree species in the Počarová area, left – autumn 2022 and right – spring 2023

4 3D-CNN MODEL ARCHITECTURE

The CNNs are deep learning models that employ filters to the raw input picture to produce a hierarchy of more complicated features. Due to this ability which extracts hierarchical features from high-dimensional data, CNNs have become increasingly popular in the field of object classification for hyperspectral images [33]. A 3D-CNN operates on the same fundamental principle as a 1D-CNN, but extends the convolution operation to three dimensions. While 1D-CNNs apply convolutional filters along a single dimension, 3D-CNNs use three-dimensional kernels that slide across the spatial and spectral dimensions of the input data. This allows the network to simultaneously capture local patterns in all three directions, enabling the extraction of joint spectral-spatial features from volumetric data such as hyperspectral image cubes [34].

The architecture of the choosen model with 17 layers is based on [35]. It can be divided into two basic parts: feature extraction (Figure 9) and classification (Figure 10).

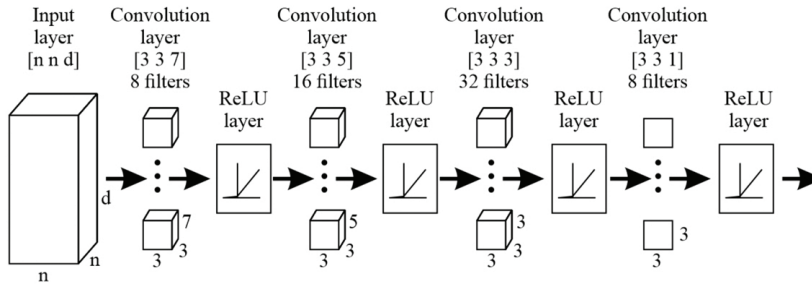

Figure 9. Feature extraction part, where n is the sliding window side and d is the number of channels

The feature extraction part begins with an input layer, to which three dimensional input samples are fed. The feature extraction process itself is performed using four consecutive 3D convolutional layers with a ReLU activation function.

The classification part of the model consists of a fully connected layer containing 256 neurons with a ReLU activation function, followed by a dropout layer with a probability of 0.4 that a given neuron will be randomly set to zero in a given iteration. The next layer is a fully connected layer with 128 neurons, followed by another dropout layer with a probability of 0.4. The last fully connected layer has a number of neurons equal to the number of classes c with a softmax activation function, and the final layer is a classification layer, the size of which is also given by the number of classification classes c.

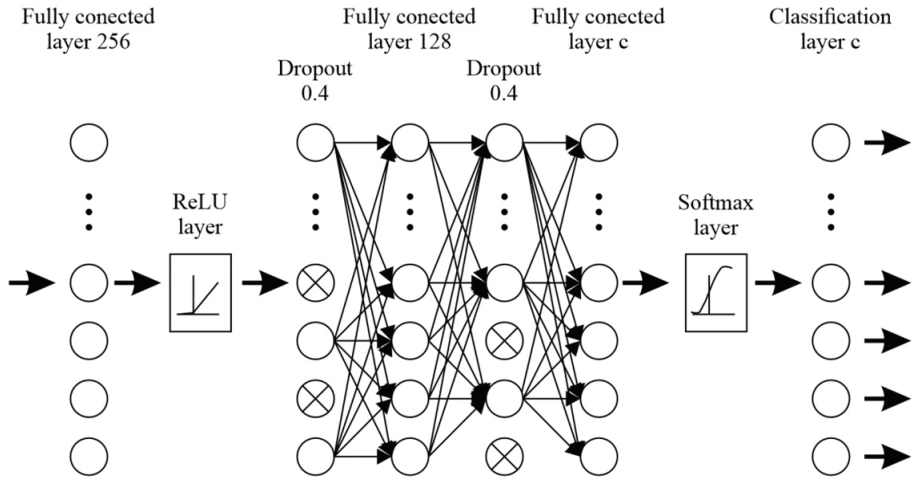

Figure 10. Classification part, where c is number of classes

5 EXPERIMENTS

Our main criterion was to minimize the input size of hyperspectral data, which means finding the minimum number of principal components and also minimizing the size of the sliding window (SW) while maintaining the required level of accuracy. Another criterion is reducing computational complexity without affecting the classification results. In order to achieve these criteria, data preprocessing was applied, consisting of three phases: reduction of the dimension of the input feature space, adjustment of the data set, and adjustment of the image size of the area after applying the SW.

5.1 Data Preprocessing

The first phase was to reduce the dimension of the input feature space. The reduction itself was performed by extracting features using PCA. The main goal of feature extraction was to achieve the best possible classification results with the 3D-CNN model, using a custom dataset and a pre-existing network architecture.

The second phase was dataset adjustment. The data for each area consisted of a varying number of samples and their corresponding classes. One sample of the input image was represented by a SW with resolution r:

$$r = n \times n \times d, \tag{1}$$

where n represents the side length of the square forming the SW and d is the dimensionality of the features corresponding to a single pixel. The number of SW

O for an image of a given area is therefore determined by the first two dimensions of the hyperspectral image:

$$O = M \times N, \tag{2}$$

where M and N are the sizes of the first two dimensions of the hyperspectral image, where O also indicates the total number of pixels in that image. Due to the uniformity of the sizes of individual windows, the image of each hyperspectral region contained padding u, where u is defined as the quotient of n divided by 2 using integer division. After applying the SW, the task is transformed into a 4-dimensional space D, where the first dimension corresponds to the number of SW O, the second and third dimensions correspond to the $n \times n$ SW raster, and the fourth dimension represents the feature dimension d:

$$D = O \times n \times n \times d. \tag{3}$$

The third phase consists of adjusting the image size of the area after applying the SW. The size reduction is performed by selecting windows that belong to one of the classes. This gives us the final image, which is the template for the input samples, i.e., 3D SW (Figure 11). Subsequently, the sets were divided into training, validation, and testing subsets, with a ratio of 60:10:30.

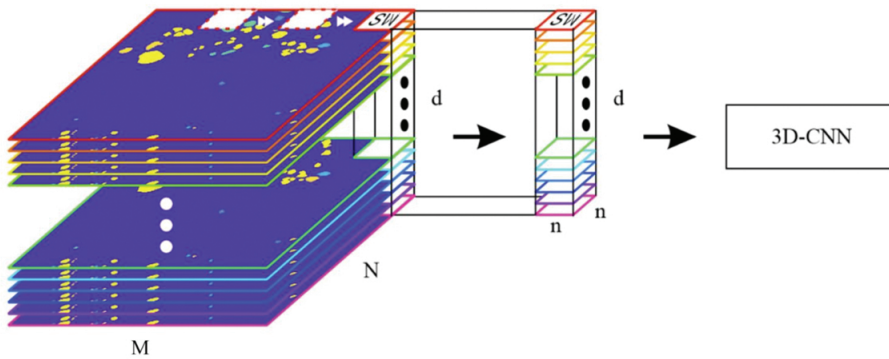

Figure 11. 3D-CNN input

5.2 Training and Testing

The hyperparameters of the selected 3D-CNN model were chosen based on a number of experiments within the range specified in Table 2. Testing was performed on two input window sizes. The first was a window from the lower boundary with dimensions $9 \times 9 \times d$, which represented the smallest possible input window size for the selected neural network model, and the second was a window with dimensions $15 \times 15 \times d$. An odd-sized window was required to ensure a clearly defined central pixel

and a symmetric neighborhood. While the $9 \times 9 \times d$ window represents the smallest possible size, the $15 \times 15 \times d$ window was selected to capture a wider spatial context. Larger window sizes were not used, as they would cover entire tree groups, leading to excessive overlap and reduced sensitivity to local spatial variations. Window sizes of $11 \times 11 \times d$ and $13 \times 13 \times d$ were tested; however, they are not reported in this paper because they negligibly changed the results.

Parameter	**Selection Interval**	**Selected Value**
Number of epochs	50–200	200
Mini batch size	128–512	256
Initial learning rate	0.01–0.00001	0.0001
Momentum	0.9	0.9
Learning rate factor	0.1–0.001, none	none
Optimization algorithm	ADAM	ADAM
Learning rate schedule	Piecewise, none	none
Learning rate drop period	30–100, none	none
Gradient threshold method	l2norm	l2norm
Gradient threshold	0.01	0.01
Validation frequency	50–200 iterations	100 iterations
Validation patience	4–6	5
Output network	Best validation loss	Best validation loss

Table 2. Hyperparameter selection

6 RESULTS

We present a comparison of the outputs of 3D-CNN classification of hyperspectral data from the autumn and spring collections for the individual areas of Visolaje, Počarová and Sverepec, as well as a comparison of the classification of fused data from the autumn collection of all three areas using the 3D-CNN model and the 1D-CNN model. These experiments aim to assess the 3D-CNN model on individual autumn and spring datasets for each area, and to compare its performance with a 1D-CNN on the fused autumn dataset, highlighting the advantages of capturing spatial-spectral correlations in hyperspectral data.

6.1 3D-CNN Classification of Autumn and Spring Collections Comparison

The results shown in Tables 3 and 4 demonstrate that, for the autumn model, a SW size of $15 \times 15 \times d$ outperformed the $9 \times 9 \times d$ window, with an average improvement of 0.0117 in classification accuracy and 0.0139 in the kappa score. For the spring model, the $15 \times 15 \times d$ window also achieved the best results, with an average classification accuracy improvement of 0.0178 and a kappa score increase of 0.0218. Overall, the best performance was obtained using a window size of $15 \times 15 \times 30$.

Area	Visolaje		Počarová		Sverepec	
Input Data Dimension	Accuracy	Kappa Score	Accuracy	Kappa Score	Accuracy	Kappa Score
$15 \times 15 \times 30$	0.9993	0.9992	0.9966	0.9959	0.9992	0.9989
$15 \times 15 \times 20$	0.9979	0.9973	0.9959	0.9951	0.9989	0.9985
$15 \times 15 \times 15$	0.9977	0.9971	0.993	0.9916	0.9982	0.9976
$15 \times 15 \times 13$	0.998	0.9975	0.9901	0.9882	0.9984	0.9979
$9 \times 9 \times 30$	0.9957	0.9946	0.9904	0.9885	0.999	0.9987
$9 \times 9 \times 20$	0.9927	0.9941	0.9815	0.9779	0.9953	0.9939
$9 \times 9 \times 15$	0.9865	0.9832	0.9595	0.9516	0.9925	0.9902
$9 \times 9 \times 13$	0.9875	0.9844	0.9484	0.9383	0.9938	0.9919

Table 3. Classification results for hyperspectral data from the autumn collection

Area	Visolaje		Počarová		Sverepec	
Input Data Dimension	Accuracy	Kappa Score	Accuracy	Kappa Score	Accuracy	Kappa Score
$15 \times 15 \times 30$	0.9994	0.9993	0.9963	0.9954	0.9992	0.999
$15 \times 15 \times 20$	0.9994	0.9993	0.9963	0.9954	0.9986	0.9982
$15 \times 15 \times 15$	0.9986	0.9984	0.989	0.9866	0.9979	0.9974
$15 \times 15 \times 13$	0.998	0.9977	0.9915	0.9897	0.9966	0.9957
$9 \times 9 \times 30$	0.9986	0.9983	0.9876	0.9849	0.9982	0.9976
$9 \times 9 \times 20$	0.9901	0.9883	0.9751	0.9696	0.9963	0.9953
$9 \times 9 \times 15$	0.9865	0.9841	0.9337	0.9187	0.9933	0.9914
9x9x13	0.9662	0.9601	0.9369	0.9228	0.9844	0.98

Table 4. Classification results for hyperspectral data from the spring collection

For this reason, we further analyze models with a comparable results and smaller SW size to the model with a SW with a size of $15 \times 15 \times d$, as the window $15 \times 15 \times d$ showed minimal changes even when using the lowest number of principal components. Comparable results were achieved for some areas with a SW size of $9 \times 9 \times 20$. However, when using 20 principal components, some sections of spring Počarová exhibited the incorrect classification of almost entire groups of trees. Consequently, the $9 \times 9 \times 30$ window was included in the analysis as an additional comparable configuration. For the purpose of this comparison, Figures 12, 13 and 14 illustrate the classification results for individual areas in autumn 2022 and spring 2023 obtained with a SW of $9 \times 9 \times 30$.

For both the autumn and spring models, average accuracy for a SW with a size of $9 \times 9 \times 30$ was 0.995. Kappa score reached an average of 0.994. Overall, the classification accuracy is high across all analyzed models. However, upon closer inspection, the $9 \times 9 \times 30$ model differs from the $15 \times 15 \times d$ models in that it struggles to correctly classify edge pixels located at the boundaries of tree groups, as illustrated in the figures, where the grayscale pixels indicate correctly classified pixels, with different shades representing different classes, while the colored pixels

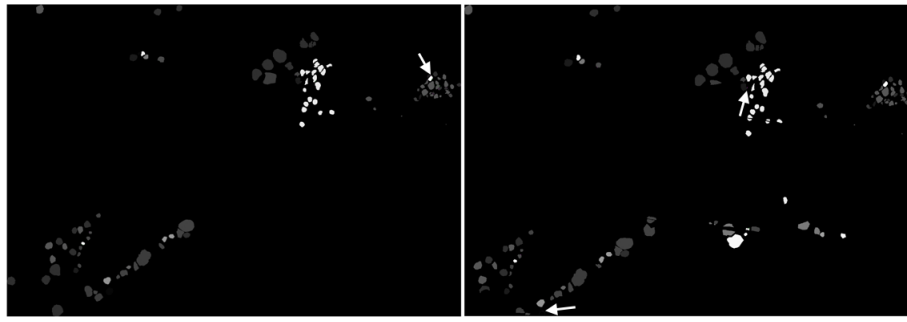

Figure 12. Visolaje area $9 \times 9 \times 30$, left – autumn 2022, right – spring 2023

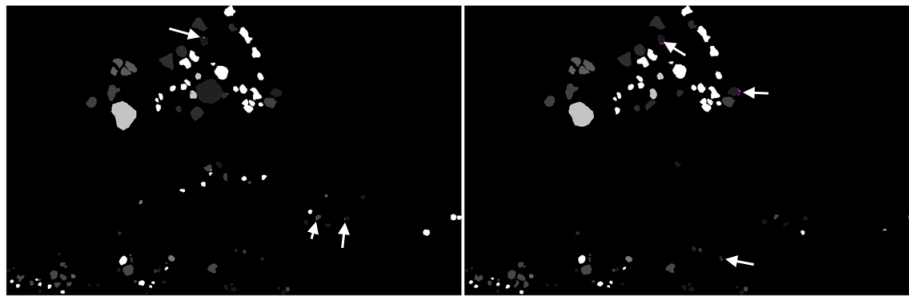

Figure 13. Počarová area $9 \times 9 \times 30$, left – autumn 2022, right – spring 2023

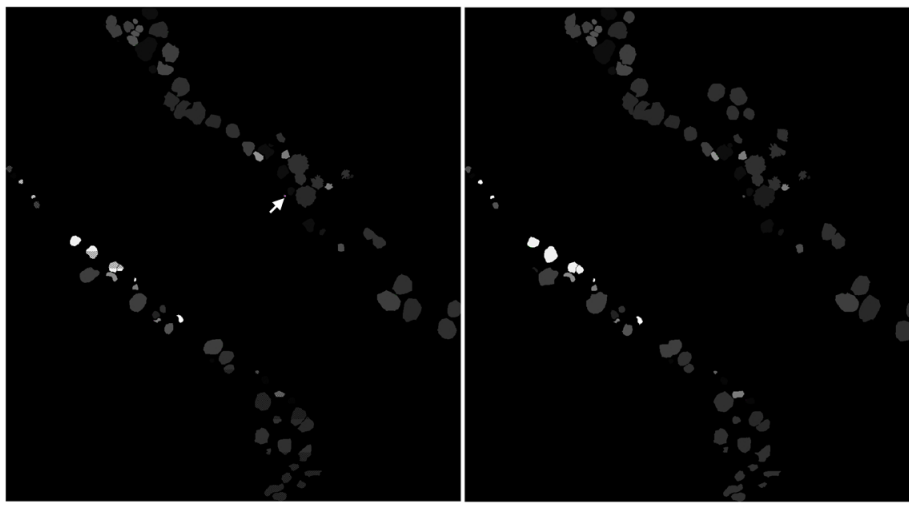

Figure 14. Sverepec area $9 \times 9 \times 30$, left – autumn 2022, right – spring 2023

highlight incorrectly classified pixels (also indicated with an arrow). This is likely due to the less distinct spectral-spatial characteristics of these boundary pixels, which makes them more difficult to assign to the correct class. This is most evident in the Počarová area (Figure 13), which, probably due to insufficient representation of misclassified classes, achieved slightly worse results than Sverepec and Visolaje. The spring models also show lower classification performance, likely due to seasonal changes that affect the spectral characteristics of the trees.

6.2 3D-CNN and 1D-CNN Classification Results Comparison

Based on the results presented in Section 6.1, we fused all three areas of the autumn collection into one for comparison with our previous study [32] in order to compare pixel and object classification. This study evaluated pixel-based classification using a 1D-CNN (Table 5). Autumn data from three selected locations were compared. A comparison of these two approaches suggests that the classification results using 3D-CNN improved by at least 9 %. Neighboring pixels therefore have a significant impact on the classification results of hyperspectral data of tree structures.

Area	1D-CNN $1 \times 1 \times 50$		3D-CNN $9 \times 9 \times 30$		3D-CNN $15 \times 15 \times 13$	
	Classif. Accuracy	Kappa Score	Classif. Accuracy	Kappa Score	Classif. Accuracy	Kappa Score
Visolaje	0.893	0.872	0.989	0.986	0.988	0.986
Sverepec	0.919	0.898	0.993	0.992	0.995	0.993
Počarová	0.851	0.813	0.988	0.985	0.993	0.992
All areas	0.857	0.836	0.980	0.976	0.932	0.919

Table 5. 1D-CNN and 3D-CNN comparison

7 CONCLUSION

In this article, we present the classification of a custom hyperspectral dataset of tree species using a 3D-CNN model. The quality of the dataset was evaluated using data from spring and autumn collections across three different areas located near power transmission lines in Slovakia. The classification results highlight the importance of seasonal climatic conditions under which the data are collected. The autumn collection achieved better performance, particularly in the classification of edge pixels at the boundaries of tree groups in the hyperspectral images, which tend to exhibit mixed spectral characteristics, probably due to overlaps with other trees. We further investigated autumn data using both 3D-CNN and 1D-CNN models, enabling a comparison between object-based and pixel-based classification approaches. The results clearly demonstrate that object-based classification achieves higher classification accuracy and kappa scores compared to pixel-based classification, and performs significantly better in areas with lower sample representation for individual tree

species. This suggests that, in addition to purely spectral information, spatial characteristics play a crucial role, mainly when classifying non-iid data. One of the main advantages of the selected model is its high classification accuracy across different areas in both spring and autumn conditions. Another advantage is the model's ability to directly analyze and classify hyperspectral data containing radiance values. Despite the promising results, the proposed approach has several limitations. The model was trained and evaluated on data from a limited number of areas, which restricts its ability to generalize to unseen environments with different vegetation structures, acquisition conditions, or seasonal characteristics. In addition, the reliance on fixed SW sizes can limit the model's adaptability to varying spatial scales, particularly in heterogeneous forest regions. The performance of the model is also influenced by the availability and quality of labelled training data, which may be difficult to obtain in real-world scenarios. Furthermore, the proposed approach was evaluated under controlled experimental conditions, and its application to large-scale or operational settings may require additional adjustments, such as model re-training, domain adaptation strategies, or integration with complementary data sources. Future work will focus on adapting and generalizing the model to enable cross-area classification, as well as the identification of previously unseen tree species and structures.

Acknowledgement

This work was supported by the Slovak Scientific Grant Agency VEGA No. 2/0081/26, by the Slovak Research and Development Agency APVV-20-0548 (ARIEN) and by the EU NextGenerationEU through the Recovery and Resilience Plan for Slovakia under the project No. 09I05-03-V02-00055 (DICRIS).

REFERENCES

[1] Patro, R. N.—Subudhi, S.—Biswal, P. K.—Dell'acqua, F.: A Review of Unsupervised Band Selection Techniques: Land Cover Classification for Hyperspectral Earth Observation Data. IEEE Geoscience and Remote Sensing Magazine, Vol. 9, 2021, No. 3, pp. 72–111, doi: 10.1109/MGRS.2021.3051979.

[2] Khan, M. J.—Khan, H. S.—Yousaf, A.—Khurshid, K.—Abbas, A.: Modern Trends in Hyperspectral Image Analysis: A Review. IEEE Access, Vol. 6, 2018, pp. 14118–14129, doi: 10.1109/ACCESS.2018.2812999.

[3] Kang, Z.—Liao, Y.—Yang, X.—Li, Z.: A VCA Combined MHSA-CNN for Aero-Engine Hot Jet Remote Sensing Mixed Spectral Feature Extraction. Remote Sensing, Vol. 17, 2025, No. 7, Art. No. 1147, doi: 10.3390/rs17071147.

[4] Sawant, S. S.—Manoharan, P.—Loganathan, A.: Band Selection Strategies for Hyperspectral Image Classification Based on Machine Learning and Artificial Intelligent Techniques – Survey. Arabian Journal of Geosciences, Vol. 14, 2021, No. 7, Art. No. 646, doi: 10.1007/s12517-021-06984-w.

[5] Chen, X.—Ke, J.—Zhang, Y.—Liu, L.—Lu, W.—Jing, S.—Zhang, X.—Guo, X.—Shen, A.: Multiple Features Extraction and Fusion for Ultrasound Dynamic Images Classification. Computing and Informatics, Vol. 43, 2024, No. 6, pp. 1455–1482, doi: 10.31577/cai_2024_6_1455.

[6] Vaddi, R.—Prabukumar, M.: Comparative Study of Feature Extraction Techniques for Hyper Spectral Remote Sensing Image Classification : A Survey. 2017 International Conference on Intelligent Computing and Control Systems (ICICCS), 2017, pp. 543–548, doi: 10.1109/ICCONS.2017.8250521.

[7] Ahmad, M.—Shabbir, S.—Roy, S. K.—Hong, D.—Wu, X.—Yao, J.—Khan, A. M.—Mazzara, M.—Distefano, S.—Chanussot, J.: Hyperspectral Image Classification – Traditional to Deep Models: A Survey for Future Prospects. IEEE Journal of Selected Topics in Applied Earth Observations and Remote Sensing, Vol. 15, 2022, pp. 968–999, doi: 10.1109/JSTARS.2021.3133021.

[8] Li, X.—Li, Z.—Qiu, H.—Hou, G.—Fan, P.: An Overview of Hyperspectral Image Feature Extraction, Classification Methods and the Methods Based on Small Samples. Applied Spectroscopy Reviews, Vol. 58, 2023, No. 6, pp. 367–400, doi: 10.1080/05704928.2021.1999252.

[9] Sun, W.—Du, Q.: Hyperspectral Band Selection: A Review. IEEE Geoscience and Remote Sensing Magazine, Vol. 7, 2019, No. 2, pp. 118–139, doi: 10.1109/MGRS.2019.2911100.

[10] Hennessy, A.—Clarke, K.—Lewis, M.: Hyperspectral Classification of Plants: A Review of Waveband Selection Generalisability. Remote Sensing, Vol. 12, 2020, No. 1, Art. No. 113, doi: 10.3390/rs12010113.

[11] Ong, P.—Chiu, S. Y.—Tsai, I. L.—Kuan, Y. C.—Wang, Y. J.—Chuang, Y. K.: Nondestructive Egg Freshness Assessment Using Hyperspectral Imaging and Deep Learning with Distance Correlation Wavelength Selection. Current Research in Food Science, Vol. 11, 2025, Art. No. 101133, doi: 10.1016/j.crfs.2025.101133.

[12] Sawant, S. S.—Prabukumar, M.: A Survey of Band Selection Techniques for Hyperspectral Image Classification. Journal of Spectral Imaging, Vol. 9, 2020, Art. No. a5, doi: 10.1255/jsi.2020.a5.

[13] Li, Z.—Zhao, B.—Wang, W.: An Efficient Spectral Feature Extraction Framework for Hyperspectral Images. Remote Sensing, Vol. 12, 2020, No. 23, Art. No. 3967, doi: 10.3390/rs12233967.

[14] Anand, R.—Veni, S.—Geetha, P.—Rama Subramoniam, S.: Extended Morphological Profiles Analysis of Airborne Hyperspectral Image Classification Using Machine Learning Algorithms. International Journal of Intelligent Networks, Vol. 2, 2021, pp. 1–6, doi: 10.1016/j.ijin.2020.12.006.

[15] Zhou, L.—Ma, X.—Wang, X.—Hao, S.—Ye, Y.—Zhao, K.: Shallow-to-Deep Spatial–Spectral Feature Enhancement for Hyperspectral Image Classification. Remote Sensing, Vol. 15, 2023, No. 1, Art. No. 261, doi: 10.3390/rs15010261.

[16] Zhang, J.—Zheng, R.—Chen, X.—Hong, Z.—Li, Y.—Lu, R.: Spectral Correlation and Spatial High–Low Frequency Information of Hyperspectral Image Super-Resolution Network. Remote Sensing, Vol. 15, 2023, No. 9, Art. No. 2472, doi:

10.3390/rs15092472.

[17] Wu, J.—Sun, X.—Qu, L.—Tian, X.—Yang, G.: Learning Spatial–Spectral-Dimensional-Transformation-Based Features for Hyperspectral Image Classification. Applied Sciences, Vol. 13, 2023, No. 14, Art. No. 8451, doi: 10.3390/app13148451.

[18] Kumar, B.—Dikshit, O.—Gupta, A.—Singh, M. K.: Feature Extraction for Hyperspectral Image Classification: A Review. International Journal of Remote Sensing, Vol. 41, 2020, No. 16, pp. 6248–6287, doi: 10.1080/01431161.2020.1736732.

[19] Gao, P.—Wang, J.—Zhang, H.—Li, Z.: Boltzmann Entropy-Based Unsupervised Band Selection for Hyperspectral Image Classification. IEEE Geoscience and Remote Sensing Letters, Vol. 16, 2019, No. 3, pp. 462–466, doi: 10.1109/LGRS.2018.2872358.

[20] Yu, W.—Zhang, M.—Shen, Y.: Combined FATEMD-Based Band Selection Method for Hyperspectral Images. IET Image Processing, Vol. 13, 2019, No. 2, pp. 287–298, doi: 10.1049/iet-ipr.2018.5550.

[21] Du, X.—Chen, H.—Liu, Z.—Yang, C.: A Novel Unsupervised Bands Selection Algorithm for Hyperspectral Image. Optik, Vol. 158, 2018, pp. 985–996, doi: 10.1016/j.ijleo.2018.01.001.

[22] Sawant, S.—Manoharan, P.: Hyperspectral Band Selection Based on Metaheuristic Optimization Approach. Infrared Physics & Technology, Vol. 107, 2020, Art. No. 103295, doi: 10.1016/j.infrared.2020.103295.

[23] Wang, M.—Wu, C.—Wang, L.—Xiang, D.—Huang, X.: A Feature Selection Approach for Hyperspectral Image Based on Modified Ant Lion Optimizer. Knowledge-Based Systems, Vol. 168, 2019, pp. 39–48, doi: 10.1016/j.knosys.2018.12.031.

[24] Morales, G.—Sheppard, J. W.—Logan, R. D.—Shaw, J. A.: Hyperspectral Dimensionality Reduction Based on Inter-Band Redundancy Analysis and Greedy Spectral Selection. Remote Sensing, Vol. 13, 2021, No. 18, Art. No. 3649, doi: 10.3390/rs13183649.

[25] Medjahed, S. A.—Ouali, M.: Band Selection Based on Optimization Approach for Hyperspectral Image Classification. The Egyptian Journal of Remote Sensing and Space Science, Vol. 21, 2018, No. 3, pp. 413–418, doi: 10.1016/j.ejrs.2018.01.003.

[26] Raczko, E.—Zagajewski, B.: Tree Species Classification of the UNESCO Man and the Biosphere Karkonoski National Park (Poland) Using Artificial Neural Networks and APEX Hyperspectral Images. Remote Sensing, Vol. 10, 2018, No. 7, Art. No. 1111, doi: 10.3390/rs10071111.

[27] Gao, J.—Zhao, L.—Li, J.—Deng, L.—Ni, J.—Han, Z.: Aflatoxin Rapid Detection Based on Hyperspectral with 1D-Convolution Neural Network in the Pixel Level. Food Chemistry, Vol. 360, 2021, Art. No. 129968, doi: 10.1016/j.foodchem.2021.129968.

[28] Zhou, J.—Zeng, S.—Xiao, Z.—Zhou, J.—Li, H.—Kang, Z.: An Enhanced Spectral Fusion 3D CNN Model for Hyperspectral Image Classification. Remote Sensing, Vol. 14, 2022, No. 21, Art. No. 5334, doi: 10.3390/rs14215334.

[29] Liu, Z.—Wang, W.—Ma, Q.—Liu, X.—Jiang, J.: Rethinking 3D-CNN in Hyperspectral Image Super-Resolution. Remote Sensing, Vol. 15, 2023, No. 10,

Art. No. 2574, doi: 10.3390/rs15102574.

[30] Salas, E. A. L.—Subburayalu, S. K.: Modified Shape Index for Object-Based Random Forest Image Classification of Agricultural Systems Using Airborne Hyperspectral Datasets. PLoS ONE, Vol. 14, 2019, No. 3, Art. No. e0213356, doi: 10.1371/journal.pone.0213356.

[31] Badidová, B.—Forgáč, R.—Očkay, M.—Javurek, M.—Krammer, P.—Hluchý, L.: A Dual-Camera Analysis of PCA Coefficients for Hyperspectral Classification of Tree Species. 2025 Cybernetics & Informatics (K&I), 2025, pp. 1–5, doi: 10.1109/KI64036.2025.10916439.

[32] Forgáč, R.—Badidová, B.—Očkay, M.—Krammer, P.—Javurek, M.—Biľanská, M.: Contribution to Pixel-Based Hyperspectral Classification of Tree Species by 1D-CNN. 2023 Communication and Information Technologies (KIT), 2023, pp. 1–5, doi: 10.1109/KIT59097.2023.10297026.

[33] Islam, M. T.—Islam, M. R.—Uddin, M. P.—Ulhaq, A.: A Deep Learning-Based Hyperspectral Object Classification Approach via Imbalanced Training Samples Handling. Remote Sensing, Vol. 15, 2023, No. 14, Art. No. 3532, doi: 10.3390/rs15143532.

[34] Zhang, H.—Tu, K.—Lv, H.—Wang, R.: Hyperspectral Image Classification Based on 3D–2D Hybrid Convolution and Graph Attention Mechanism. Neural Processing Letters, Vol. 56, 2024, No. 2, Art. No. 117, doi: 10.1007/s11063-024-11584-2.

[35] Statistics and Machine Learning Toolbox. The MathWorks Inc., Natick, Massachusetts, United States, 2022, `https://www.mathworks.com/help/stats/index.html`.

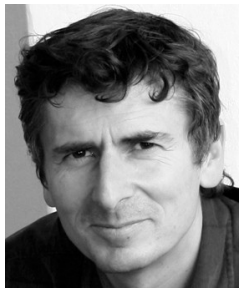

Radoslav Forgáč is Associate Professor and research scientist at the Institute of Informatics, Slovak Academy of Sciences, and a university teacher at the Department of Informatics at the Armed Forces Academy in Liptovský Mikuláš. He received his Ph.D. in artificial intelligence from the Technical University of Košice. His research focuses on artificial intelligence, with an emphasis on the analysis and visualization of multidimensional data, image steganography and classification, regression, and predictive modeling.

Bianca Badidová is a Ph.D. candidate at the Department of Informatics at the Armed Forces Academy in Liptovský Mikuláš. She participates in scientific projects at the Institute of Informatics of the Slovak Academy of Sciences. Her research focuses on data analysis, cybersecurity, and neural networks.

Miloš Očkay is a Researcher at the Institute of Informatics, Slovak Academy of Sciences and Associate Professor at the Department of Informatics at the Armed Forces Academy in Liptovský Mikuláš. He holds his Ph.D. in informatics, received in 2012 from the Technical University of Košice. His research focuses on parallel computing and neural networks.

Martin Javurek is Assistant Professor at the Department of Informatics at the Armed Forces Academy in Liptovský Mikuláš and a Researcher at the Institute of Informatics, Slovak Academy of Sciences. He holds his Ph.D. in informatics, earned in 2017 from the Armed Forces Academy in Liptovský Mikuláš. His research focuses on neural networks, cybersecurity and cryptography.

Ladislav Hluchý is Associate Professor, senior researcher and the Head of the Department of Parallel and Distributed Information Processing at the Institute of Informatics, Slovak Academy of Sciences. He has been active in European research programs since FP4 and has led the II SAS team in dozens of research projects in FP4, FP5, FP6, FP7, H2020, and HE. During his research career, he authored over 150 scientific publications. His specialization is distributed information processing, cloud computing and data science.

Ľuboš Skurčák graduated from the Faculty of Electrical Engineering and Information Technology at the Slovak University of Technology in Bratislava in 1999, earning his M.Sc. in power engineering. Since 1999, he has been working at VUJE, a.s., in field support and the operation of transmission and distribution systems. He obtained his Ph.D. degree in 2015 from the same faculty. He has more than 20 years of experience in industrial research and experimental development in power engineering, focusing on the assessment, reliability, and development of transmission and distribution networks. In recent years, his work has focused on remote sensing applications, including the application of AI to process LiDAR and hyperspectral data for monitoring and condition assessment of overhead power lines. He is a long-standing member of CIGRE, and author or co-author of several technical publications.